Mechanistic Investigations into the Selective Reduction of Oxygen by a MCO T3 site-inspired Copper Complex

Phebe H. van Langevelde[a#], Errikos Kounalis[b#], Lars Killian[b#], Emily C. Monkcom[b], Daniël L. J. Broere[b*], and Dennis G. H. Hetterscheid[a*]

[a]Leiden Institute of Chemistry, Leiden University, 2300 RA, Leiden (The Netherlands). Email: d.g.h.hetterscheid@chem.leidenuniv.nl

[b]Organic Chemistry and Catalysis, Institute for Sustainable and Circular Chemistry, Faculty of Science, Utrecht University, Universiteitsweg 99, 3584 CG, Utrecht (The Netherlands). Email: d.l.j.broere@uu.nl

[#]These authors contributed equally

Abstract

Understanding how multicopper oxidases (MCOs) efficiently and selectively reduce oxygen in the trinuclear copper cluster (TNC) is of great importance. Previously it was reported that when the T2-site is removed from the TNC, all O_2 binding activity at the dinuclear T3-site is lost. Computational studies attribute this loss of activity to the flexibility of the protein active site, where the T3-copper centers move apart to minimize electrostatic repulsions. To address the question if and how a more constrained T3-site will catalyze the reduction of oxygen, we herein report a mechanistic investigation into the oxygen reduction reaction (ORR) activity of the dinuclear copper complex **$[Cu_2L(\mu\text{-}OH)]^{3+}$** (**L**=2,7-bis[bis(2-pyridylmethyl)aminomethyl]-1,8-naphthyridine). This T3-inspired complex confines the Cu centers in a rigid scaffold in close proximity instead of the flexible scaffold found in the protein active site and we demonstrate that under these constraints the dinuclear copper site displays ORR activity. Compared to the ORR mechanism of MCOs, we show that electrochemical reduction of **$[Cu_2L(\mu\text{-}OH)]^{3+}$** follows a similar pathway as the reduction of the resting enzyme due to the presence of the Cu-OH-Cu motif. By identification of key intermediates along the catalytic cycle of **$[Cu_2L(\mu\text{-}OH)]^{3+}$** we provide for the first time evidence that metal-metal cooperativity takes place during electrocatalysis of the ORR by a copper-based catalyst, which is achieved by the ability of the rigid ligand framework to bind two copper atoms in close proximity. Electrochemical studies show that the mechanisms of the ORR and hydrogen peroxide reduction reaction (HPRR) found for **$[Cu_2L(\mu\text{-}OH)]^{3+}$** are different from the ones found for analogous mononuclear copper catalysts. In addition, the metal-metal cooperativity results in an improved selectivity for the four-electron ORR of more than 70%. This selectivity is achieved by better stabilization of reaction intermediates between both copper centers, which is also essential for the ORR mechanism observed in MCOs. Overall, the mechanism of the **$[Cu_2L(\mu\text{-}OH)]^{3+}$**-catalyzed ORR in this work gives insight into the ORR activity of a T3-site and contributes to understanding of how the ORR activity and selectivity are established in MCOs.

Introduction

The four-electron reduction of oxygen to water plays a key role in fuel cell technology.[1, 2] Currently, the most efficient catalysts for the oxygen reduction reaction (ORR) are Pt-based, which drives up the costs of fuel cell devices and limits their commercial viability.[3-5] Nature has found an efficient way to reduce oxygen in multicopper oxidases (MCOs) using earth-abundant copper.[6] The thermodynamic and kinetic properties of the ORR catalyzed by MCOs have been compared to those of Pt electrodes.[7-9] Interestingly, immobilization of the MCO enzyme laccase on electrodes resulted in the selective four-electron reduction of oxygen to water at a lower overpotential than Pt. From this it is apparent that MCOs, especially laccases, are excellent ORR catalysts. Understanding how these MCOs achieve these remarkable activities on a chemical level can point scientists towards new design principles for the next generation ORR catalysts, assisting the energy transition the world is currently facing.

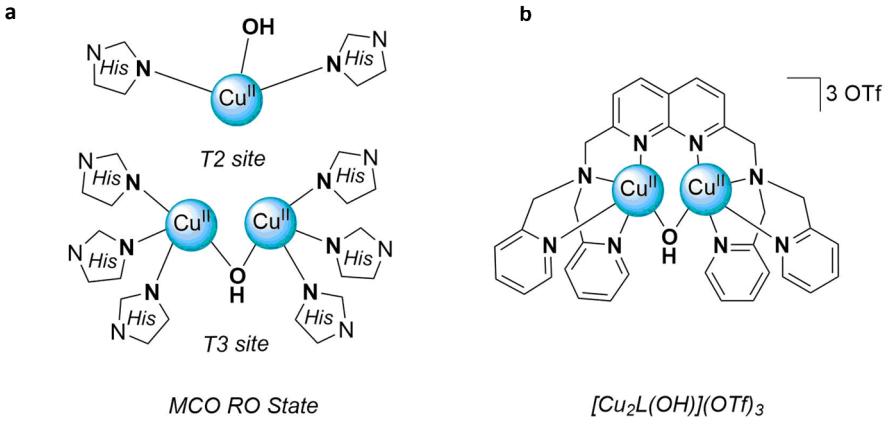

Figure 1 Schematic overview of **a)** the MCO active site in the RO state, histidines simplified for clarity and **b)** Structure of the **[Cu_2L(μ-OH)](OTf)$_3$** complex.

MCOs are a class of enzymes that couple the oxidation of a variety of substrates to the reduction of oxygen.[6] The MCO active site consists of a mononuclear T1 copper site and the trinuclear copper cluster (TNC) containing the bimetallic T3 and mononuclear T2 sites (**Figure 1a**).[10] The T1 site is responsible for the oxidation of substrates and the transfer of electrons to the TNC, where in turn oxygen can bind and is reduced. A combination of spectroscopic and crystallographic studies, supported by computational studies in more recent years, have contributed to the identification of the key intermediates in the catalytic cycle.[11, 12] In addition, an overall mechanism for the four-electron reduction of oxygen was formulated involving these intermediates (**Figure 2**).[11-13]

The O_2 reduction mechanism to H_2O comprises of two distinct two-electron transfers. The first two electrons are transferred when dioxygen binds to the fully reduced (FR) state. In studies using MCOs without T1 sites or with T1 sites replaced by Hg^{2+}, the peroxide intermediate (PI), formed after this initial electron transfer, could be detected.[14-16] Supported by computational studies, the electronic structure of the PI state with a μ_3-1,1,2-peroxo ligand was elucidated.[17] In MCOs with an intact T1 site, the PI cannot be isolated since a rapid, second two-electron transfer will lead to cleavage of the O-O bond and the formation of the native intermediate (NI) state.[16] In the NI state one oxygen atom is present as μ_3-O, the other as a μ-OH between the T3 coppers.[18, 19] To complete the catalytic cycle, the NI is re-reduced to the FR state in a process involving 4 protons and 3 electrons.[20] Outside of this catalytic cycle lies the enzyme's resting oxidized (RO) state, to which the NI will slowly decay in the absence of reducing equivalents.[21, 22]

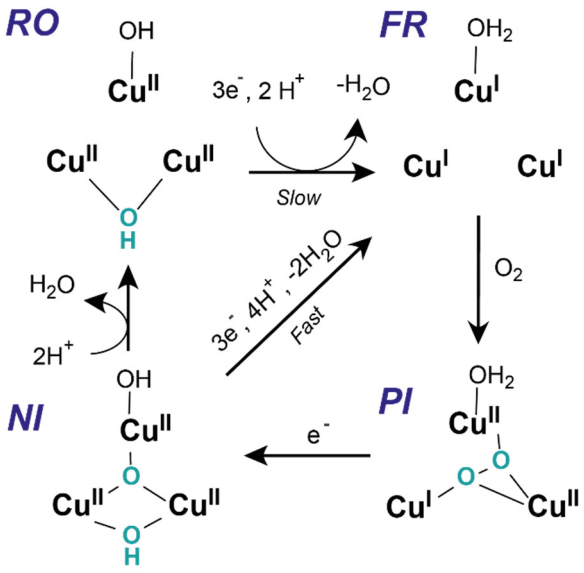

Figure 2 Schematic overview of the oxygen reduction mechanism in the TNC of MCOs.

Apparent from this mechanism is that in all catalytic intermediates, except the FR, oxygen-derived species bound between multiple copper centers play a key role. Equally, all three coppers contribute to the bridged binding of the μ_3-1,1,2-peroxo intermediate, which is essential for the reductive cleavage of the O–O bond, and the selective 4-electron reduction of oxygen.[17] In addition, the μ_3-O that forms between all coppers in the NI state is required for the fast re-reduction of the catalyst, taking place at a rate of >700 s^{-1}, as the highly basic μ_3-oxo ligand is easily protonated and reduced.[21] In contrast, the less basic nature of the Cu-OH-Cu motif in the T3 site of the RO state results in intramolecular electron transfer from the T1 site to TNC of only 0.11 s^{-1} which illustrates why the RO state is not part of the catalytic cycle.[19, 21, 22]

To gain a better understanding of the cooperativity between the three copper centers, the role these individual sites play in establishing the activity and selectivity in MCOs has been explored. Previously, the reactivity of the individual T3 site with oxygen in T2 site depleted (T2D) MCOs was investigated.[23, 24] In these modified enzymes the active site is reminiscent of other dinuclear copper enzymes like hemocyanin and tyrosinase. In hemocyanin, the T3 site enables the reversible binding of dioxygen and in tyrosinase this binding is coupled to the hydroxylation/oxidation of tyrosine.[25] Despite the resemblance to these two oxygen-binding enzymes, the T3 site of T2D MCOs was not able to bind oxygen on its own.[23, 24]

In a computational study, the group of Solomon attributed the lack of dioxygen binding in T2D laccase to the different Cu–Cu distance found in the reduced forms of the T3 site in T2D laccase and in hemocyanin/tyrosinase.[26] In T2D laccase, the active site is more flexible and as a result the two Cu(I) centers are positioned further apart (≈6 Å) to minimize the electrostatic repulsion between the two centers. In hemocyanin/tyrosinase, the two Cu(I) centers are found in closer proximity (≈4 Å), and the resulting electrostatic repulsion destabilizes the reduced state. This destabilization drives the binding and reduction of dioxygen at the reduced T3 site in hemocyanin/tyrosinase and provides a rationale for the absence of dioxygen reduction at the T3 site of T2D laccase.[26]

The absence of ORR activity in T2D MCOs as well as the computational insights provided by the group of Solomon inspired us to investigate the activity and selectivity of an individual T3-inspired dicopper site in the absence of a third copper. Moreover, using a rigid scaffold that confines both copper atoms in close proximity could allow us to experimentally investigate the hypothesis that the lack of ORR activity in T2D MCOs is due to the large Cu-Cu separation of the reduced state and whether the T2 site has a critical effect on the activity and selectivity of the ORR.

The use of biomimetic complexes to model (part of) the active site of enzymes is a well-established, elegant approach to address questions of this nature. The MCO active site has inspired the design of many molecular copper complexes to date, typically supported by polynucleating ligands that feature multiple N-donor atoms that mimic the histidine ligands in the TNC.[27, 28] The coordination chemistry and the reactivity of Cu(I) complexes with oxygen has also been extensively studied.[27-29] In addition, trinuclear copper complexes have been developed to study the role of proton-coupled electron transfers in MCOs.[30] However, when it comes to the ORR reactivity, only a few complexes with multiple metal centers have been investigated to date. Moreover, the catalytic activity of these complexes has often been investigated in organic solvents and chemical reducing agents are typically used.[31-35] These reaction conditions do not resemble those in which the ORR activity of MCOs has been studied.

On the other hand, electrochemical studies that have reported the ORR activity of homogeneous metal complexes with two[36-38] or even three[37, 39, 40] copper atoms in aqueous solutions all lack evidence that

direct cooperativity between the copper centers takes place during catalysis. The lack of cooperativity can be explained by the fact that covalently linking copper sites will not invariably result in synergy between the metal centers. For instance, not all metal centers might participate during catalysis,[37] the copper sites can turn away from each other,[36] the catalyst can decompose during electrocatalysis,[38] or multiple copper centers in close proximity will result in a change of selectivity, but not due to direct metal-metal cooperativity.[39] An exception is a study by Yu and co-workers, in which three copper centers are forced closely together improving the selectivity of the ORR, although a full characterization of the active species and a catalytic mechanism are absent.[40]

To address our research question, we set out to study the ORR activity of a complex with a rigid ligand framework that can coordinate two copper atoms in close proximity and, in addition, to study in detail the nature of the active species along the catalytic cycle. Recently, the mononuclear Cu(tmpa) complex (tmpa= tris(2-pyridylmethyl)amine) was studied in one of our groups, and was shown to catalyze the ORR with the highest TOF reported for any homogeneous copper complex.[41] Interestingly, the dinuclear analogue of tmpa, the 2,7-bis[bis(2-pyridylmethyl)aminomethyl]-1,8-naphthyridine (**BPMAN**) ligand, can coordinate two copper atoms in close proximity to form the **$[Cu_2L(\mu\text{-}OH)]^{3+}$** (L= **BPMAN**) complex[42] and was previously reported to electrochemically catalyze the water oxidation reaction (**Figure 1b**).[43] The **BPMAN** ligand is based on the 1,8-naphthyridine scaffold, which can bind two metals in close proximity,[44, 45] and a variety of biomimetic ligands containing the 1,8-naphthyridine scaffold have been reported.[42, 46-50] It is evident from **Figure 1** that **$[Cu_2L(\mu\text{-}OH)]^{3+}$** bears similarities to the T3 site in MCOs, including the μ-OH ligand. Moreover, the Cu–Cu distance in **$[Cu_2L(\mu\text{-}OH)]^{3+}$** was reported to be 3.4 Å,[43] which is similar to the reported Cu–Cu distance in the T3 site of MCOs in the RO state of approximately 3.7 Å.[12]

In this study, we present a mechanistic investigation of the ORR catalyzed by **$[Cu_2L(\mu\text{-}OH)]^{3+}$** and provide an explanation for its activity and selectivity, which is supported by a combination of electrochemical and reactivity studies to identify the nature of the active species. In addition, by comparing our results to the previously reported mononuclear Cu(tmpa) system, the effect of the dinuclear copper core on the reaction kinetics and selectivity was explored. Combined, the study of the catalytic mechanism of this T3 site-inspired complex contributes to better understanding of the ORR activity and selectivity found in MCOs.

Results and discussion

Synthesis of [Cu_2L(μ-OH)]OTf_3

The 2,7-bis[bis(2-pyridylmethyl)aminomethyl]-1,8-naphthyridine ligand was synthesized in 64% yield using a new synthetic protocol (See Supporting Information). With the **BPMAN** ligand (**L**) in hand, crystalline [BPMANCu_2(μ-OH)]$(OTf)_3$ (**[Cu_2L(μ-OH)]OTf_3**) was prepared in a reaction with $Cu(OTf)_2$ in acetonitrile according to literature procedures with a 40% yield.[43] The paramagnetic ^{1}H-NMR spectrum of **[Cu_2L(μ-OH)]$^{3+}$** in D_2O, not reported previously, shows a set of 7 and a set of 2 of equally integrating resonances with a relative ratio of 2:1 (See **Figure S3**). This observation can be explained by the methylene protons flanking the pendant pyridines being magnetically inequivalent (set of 2) and agrees with the expected resonances of the four pyridine arms and the 1,8-naphtyridine moiety. The surprisingly sharp peaks in the paramagnetic ^{1}H-NMR spectrum of this dicopper(II) compound are most likely the result of antiferromagnetic coupling between the two Cu(II) centers, as has been observed for other hydroxo-bridged dicopper(II) complexes.[51, 52] The paramagnetic ^{1}H-NMR spectrum of the same compound in DCM-d_2 gives rise to a similar spectrum, except for an additional broad resonance at -70.8 ppm shift (See **Figure S5**). We tentatively assign this resonance to the hydroxide proton and attribute the absence of this resonance in D_2O to rapid exchange of the proton with the solvent.

*Cyclic voltammetry of **[Cu_2L(μ-OH)]$^{3+}$***

The **[Cu_2L(μ-OH)]$^{3+}$** complex was studied electrochemically in a 0.1 M phosphate buffer (PB) at pH 7, using a glassy carbon (GC) working electrode. A cyclic voltammogram (CV) under Ar atmosphere shows a single Cu^{II}/Cu^{I} redox couple with a half-wave potential ($E_{1/2}$) of 0.45 V vs. RHE (**Figure 3a**). The redox couple of **[Cu_2L(μ-OH)]$^{3+}$** is shifted towards higher potentials compared to the mono-nuclear analogue Cu(tmpa) that has a $E_{1/2}$ of 0.21 V vs. RHE under the same conditions.[41] To investigate if **[Cu_2L(μ-OH)]$^{3+}$** displays ORR activity, a CV in the presence of oxygen was recorded. Indeed, the CV showed a clear catalytic wave (**Figure 3b**). In addition to the ORR, the catalytic activity of **[Cu_2L(μ-OH)]$^{3+}$** for the hydrogen peroxide reduction reaction (HPRR) is of interest because H_2O_2 is found as a detectable intermediate in the aqueous electrochemical ORR mechanism of other copper complexes with tetradentate pyridylamine ligands that is formed after the two-electron reduction of oxygen.[36, 39, 41, 53, 54] In the presence of 1.1 mM H_2O_2, which is the same concentration as the maximum solubility of oxygen in PB, a catalytic wave was observed with a slightly earlier onset than the ORR (**Figure 3b**). As this earlier onset is only present in the first scan, we contribute this occurrence to the weak binding of H_2O_2 to the oxidized form of the catalyst, although such a species could not be detected by other techniques like NMR. As the time between the first and second scan is relatively short, this equilibrium

is not restored in between cycles and the onset shifts back to that of the ORR in subsequent scans (See **Figure S8**). The peak-shaped waves in both the ORR and HPRR voltammograms indicate the depletion of substrate during catalysis. We attribute the difference in the peak catalytic currents between the ORR and HPRR to the different diffusion rates of O_2 (1.9×10^{-5} cm^2 s^{-1}) and H_2O_2 ($0.8 - 1.4 \times 10^{-5}$ cm^2 s^{-1})[55, 56] and possible difference in electron transfer number for each of the respective reduction reactions.

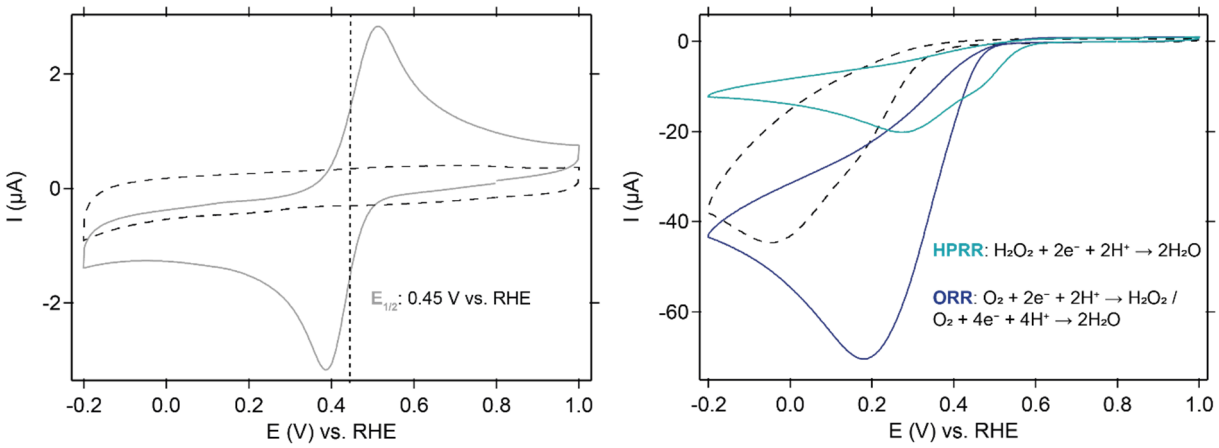

Figure 3 CVs of **a)** the Cu^{II}/Cu^{I} redox couple of **$[Cu_2L(\mu\text{-}OH)]^{3+}$** with the half-wave potential of 0.45 V vs. RHE indicated by the vertical dotted lined and the bare GC electrode under Ar atmosphere by a black dashed line, and **b)** the ORR (dark blue) and HPRR (light blue) catalysed by **$[Cu_2L(\mu\text{-}OH)]^{3+}$**. ORR activity of the bare GC electrode shown as reference (black dashed line). Conditions: 0.15 mM **$[Cu_2L(\mu\text{-}OH)]^{3+}$**, 0.1 M PB pH 7, Ar or O_2 atmosphere or 1.1 mM H_2O_2, 293 K, 100 mV/s scan rate.

Prior to further mechanistic studies, we carefully investigated if the electrochemical data is representative of the homogenous catalyst in solution, rather than any heterogeneous species that may have been deposited on the electrode surface. Such investigation on the nature and stability of the active species is important in homogeneous electrocatalysis.[57] This has been exemplified by a previous study by one of our groups on a different dicopper ORR catalyst used as a model system for MCOs, for which the sole active species in ORR was found to be copper deposit.[38] In addition, catalytic rates and selectivities can only be assigned to the homogeneous catalyst in solution if the interference of any formed heterogeneous deposits can be minimized.

To start, the possible formation of any deposited species was studied in a combination of CV experiments and electrochemical quartz crystal microbalance (EQCM) experiments (See Supporting Information section 4.1 and 4.2). First, we investigated if any species deposits onto the electrode during CV measurements, by recording a CV in a solution of **$[Cu_2L(\mu\text{-}OH)]^{3+}$**, and subsequently recording a CV of the same electrode in a solution in the absence of catalyst. These experiments under Ar atmosphere show that the **$[Cu_2L(\mu\text{-}OH)]^{3+}$** catalyst tends to adsorb onto the glassy carbon surface during CV measurements, but it is likely to stay intact as the redox couple of the species that adsorbs onto the electrode is similar to the **$[Cu_2L(\mu\text{-}OH)]^{3+}$** redox couple (See **Figure S9a, Figure S10a**). In

contrast, the same experiments in the presence of O_2 or H_2O_2 show that a new heterogeneous species forms on the electrode during catalysis that is also catalytically active for the ORR and HPRR (See **Figure S9**). Secondly, EQCM measurements were carried out to investigate the possible mass change of the electrode during CV experiments, as this is an indication that heterogeneous deposits form on the surface of the electrode. In line with the CV experiments discussed above, EQCM experiments indeed show that a heterogeneous species is formed on the surface of the electrode during catalysis, whereas this formation is prevented if the **$[Cu_2L(\mu\text{-}OH)]^{3+}$** catalyst is studied under Ar atmosphere (See **Figure S12**).

Next, we investigated to what extent the adsorption of catalyst or the formation of a heterogeneous deposit onto the electrode surface contribute to the recorded activity of **$[Cu_2L(\mu\text{-}OH)]^{3+}$**. In measurements under Ar atmosphere the adsorbed species behaves similar to homogenous one, but its catalytic activity is small as only a little amount of catalyst adsorbs (See **Figure S10**). Therefore, it was excluded that any adsorbed catalyst interferes with the measurements of the homogeneous **$[Cu_2L(\mu\text{-}OH)]^{3+}$** under Ar atmosphere.

To study if the heterogeneous deposits that form during catalysis do not contribute to the observed catalytic activity of **$[Cu_2L(\mu\text{-}OH)]^{3+}$**, measurements were carried out under non-substrate limited conditions. These conditions allow to study the catalytic activity, whilst this is not governed by the depletion of oxygen. From these measurements it is clear that the catalytic activity of **$[Cu_2L(\mu\text{-}OH)]^{3+}$** in the first scan of a CV measurement is significantly less than the activity of the deposits that form over the course of several scans (See **Figure S11**). In other words, under catalytic conditions, active deposits form over the course of multiple CV scans, but it is expected that in the first scan of any CV experiment only little amounts of deposits have formed and the largest part of the activity can be contributed to the homogeneous **$[Cu_2L(\mu\text{-}OH)]^{3+}$** species.

To ensure that the influence of any heterogeneous deposits on the results of our studies into the activity of homogeneous **$[Cu_2L(\mu\text{-}OH)]^{3+}$** is kept to a minimum, in this work only the first CV scans recorded on a freshly polished electrode were used. In addition, this study focusses solely on the fundamental catalytic mechanism of the catalyst, not on any long-term activity, since in that case the influence of heterogeneous deposits cannot be ruled out.

*Redox behavior of **$[Cu_2L(\mu\text{-}OH)]^{3+}$***

The first step in the catalytic ORR mechanism, is the reduction of **$[Cu_2L(\mu\text{-}OH)]^{3+}$** to obtain the active reduced catalyst. The redox behavior of **$[Cu_2L(\mu\text{-}OH)]^{3+}$** was previously investigated by Zhang *et al*. in 0.1 M PB of pH 7 using a boron-doped diamond (BDD) working electrode. They reported two irreversible waves for the reduction and oxidation of the catalyst with a peak-to-peak separation (ΔE_p)

of 340 mV at a scan rate of 5 mV/s. In our study, the ΔE_p of the Cu^{II}/Cu^{I} redox couple at a scan rate of 100 mV/s reduces to 127 mV (**Figure 3a**). We attribute the smaller ΔE_p in this study to the more favorable electron transfer properties of GC compared to BDD, as BDD is known to act as a semi-conductor at low dopant densities.[58]

Scan rate dependence studies of the redox couple (10-500 mV/s) show that the peak current linearly depends on the square root of the scan rate, which indicates a diffusion-controlled process and that **$[Cu_2L(\mu\text{-}OH)]^{3+}$** is present as a homogeneous species in solution (See **Figure S13b**). The ΔE_p of 127 mV at 100 mV/s indicates a quasi-reversible process and suggests that the electron transfer process to reduce and re-oxidize **$[Cu_2L(\mu\text{-}OH)]^{3+}$** is slow. In addition, a Laviron plot shows that the peak potential of the redox couple depends linearly on the logarithm of the scan rate (See **Figure S13c**), which means that the electron transfer processes in the catalyst become relatively slow compared to the timescale of the CV experiment. A third sign of slow electron transfer kinetics is the relatively low half-wave potential of the catalytic wave ($E_{cat/2}$) in the ORR and thus $E_{cat/2} < E_{1/2}$ holds for **$[Cu_2L(\mu\text{-}OH)]^{3+}$**, while for fast catalysts it is expected that $E_{cat/2} = E_{1/2}$ or even $E_{cat/2} > E_{1/2}$, when substrate depletion plays a role.

In MCOs, both copper centers in the T3 site of the RO state are reduced simultaneously in a proton-coupled electron transfer (PCET) step to form the FR state, resulting in the loss of the μ-hydroxyl ligand as H_2O.[6, 11] In this study only a single peak for the Cu^{II}/Cu^{I} redox couple is observed, which indicates that in **$[Cu_2L(\mu\text{-}OH)]^{3+}$** both copper atoms are reduced and oxidized simultaneously. To see whether the reduction of **$[Cu_2L(\mu\text{-}OH)]^{3+}$** also involves a protonation, we studied the influence of the proton concentration on the redox behavior of the complex (See supporting Information section 6). CVs of **$[Cu_2L(\mu\text{-}OH)]^{3+}$** under Ar atmosphere were recorded in a 0.1 M Na_2SO_4 electrolyte over a wide pH range and the values of $E_{1/2}$ were used to establish a Pourbaix diagram (**Figure 4)**. In this Pourbaix diagram the thermodynamically stable states of the catalyst for different pH and potential regions are identified.

In **Figure 4** the half-wave potential of **$[Cu_2L(\mu\text{-}OH)]^{3+}$** depends linearly on the pH with a slope of −28 mV/decade between pH ~4 – 7. This value is close to the theoretical value of −30 mV/decade of a PCET step in which one proton and two electrons are transferred,[59] and agrees with the simultaneous protonation of the hydroxyl ligand upon reduction of both copper centers in **$[Cu_2L(\mu\text{-}OH)]^{3+}$**. In contrast, Zhang *et al.* measured on BDD a shift of −60 mV/decade of the cathodic wave, which they contributed to the single electron reduction of **$[Cu_2L(\mu\text{-}OH)]^{3+}$** and a proton transfer forming a mixed-valence $Cu^{II}Cu^{I}$ species.[43] Our results differ from this observation, since we herein regard the redox couple measured on GC as quasi-reversible and considered the shift in $E_{1/2}$, whereas Zhang *et al.* observed an irreversible couple on BDD and instead used the shift in the cathodic wave only.

While we observe a slope in the Pourbaix diagram below pH 7, the half-wave potential does not seem to depend on the pH between pH 7 and pH 9. This points towards a mechanism in which only electrons are transferred, and the μ-hydroxyl ligand is not protonated. In the region of pH 9 and above, a slope of −27 mV/decade is observed in the Pourbaix diagram, which we ascribe to the formation of either a bis-μ-hydroxyl or deprotonated μ-O species. The slope of approximately −30 mV/decade corresponds to the simultaneous transfer of two electrons and a proton, liberating water and generating a $Cu^{I}Cu^{I}$ species.

It is important to point out that CV measurements in Na_2SO_4 electrolyte revealed that **$[Cu_2L(\mu\text{-}OH)]^{3+}$** is very sensitive to changes in pH. Both the shape and peak-to-peak separation of the redox couple change differently upon changing the pH, resulting in deviations in the Pourbaix diagram, especially around pH 8. We ascribe this irregularity to the complex's propensity to access different protonation states. Particularly, the pyridinic nitrogen atoms of the ligand can be protonated easily as shown computationally by Zhang *et al*.[43]

In addition, the redox behavior of **$[Cu_2L(\mu\text{-}OH)]^{3+}$** was studied with differential pulse voltammetry (DPV) measurements at different pH values, as this can help to identify if a chemical step takes place upon reduction or oxidation of the catalyst (See Supporting Information section 6.2). The $E_{1/2}$ values found in CV and DPV measurements differ, suggesting that one or more chemical steps precede the oxidation of the formed $Cu^{I}Cu^{I}$ species in CV experiments. This observation complicates the assignment of the species that form at different pH values. Hence, additional experiments were carried out to confirm the tentative interpretation of the Pourbaix diagram.

First, the redox measurements in 0.1 M $NaClO_4$ or 0.1 M Na_2SO_4 electrolyte resulted in a similar redox couple and pH trend, proving that the pH dependence of the **$[Cu_2L(\mu\text{-}OH)]^{3+}$** reduction is independent of the electrolyte (See **Figure S15**). In addition, the pH dependence of the redox couple and catalytic activity of **$[Cu_2L(\mu\text{-}OH)]^{3+}$** in buffered solutions show the same trend as in 0.1 M Na_2SO_4 electrolyte, with the redox couple and catalytic wave shifting towards more positive potentials in an acidic buffer (See **Figure S17**).

The redox behavior of **$[Cu_2L(\mu\text{-}OH)]^{3+}$** was also studied in acetonitrile solution, since precise control over the availability of protons is more easily attainable in organic solvent than in aqueous solution. Interestingly, a solution of 0.3 mM **$[Cu_2L(\mu\text{-}OH)]^{3+}$** in 0.1 M $TBAPF_6$ in MeCN does not show a clear reduction event, which is not in agreement with the single reduction peak observed in aqueous solutions. Addition of a proton source (triethylammonium hexafluorophosphate, $TEAPF_6$) generates a CV with a clear redox couple and a single reduction wave, demonstrating that in MeCN a proton source is required for the reduction of **$[Cu_2L(\mu\text{-}OH)]^{3+}$** (**Figure *6*a**). Such behavior is expected in organic

solutions as it is likely that upon reduction of the catalyst formation of H_2O is preferred over the liberation of OH^-. This agrees with the observations in aqueous solution below pH 7 and strongly suggests that protonation of the μ-hydroxyl ligand takes place simultaneously with reduction of the catalyst.

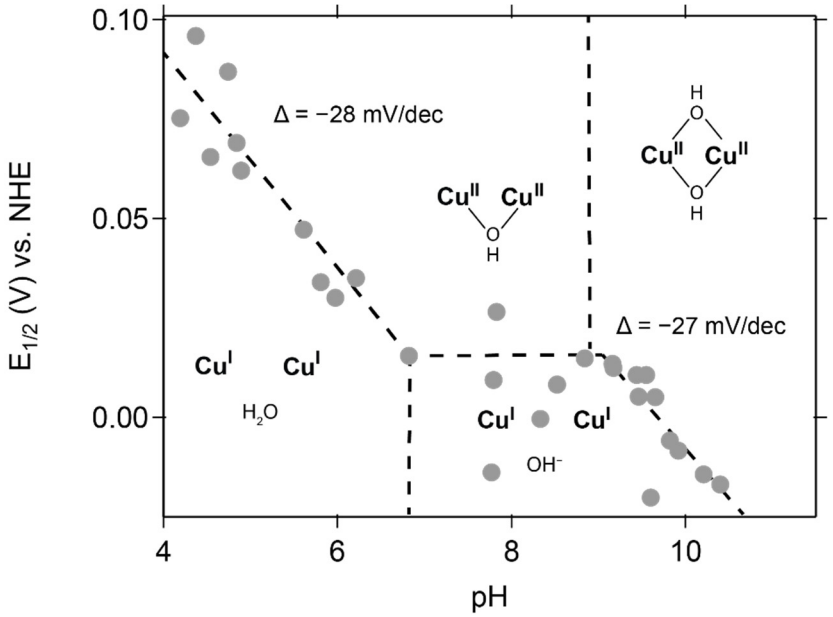

Figure 4 Pourbaix diagram of the half-wave potential of the **$[Cu_2L(\mu\text{-}OH)]^3$** redox couple as a function of pH, including the slope of the graph and the different dicopper species. Conditions: 0.15 mM **$[Cu_2L(\mu\text{-}OH)]^{3+}$**, 0.1 M Na_2SO_4, Ar atmosphere, 293 K, 100 mV/s scan rate.

The role of the bridging hydroxyl ligand

Intrigued by the complex redox behavior of **$[Cu_2L(\mu\text{-}OH)]^{3+}$**, the coordination chemistry of the Cu^{II}-OH-Cu^{II} motive was studied in more detail. To begin with, possible protonation of the μ-hydroxyl ligand was studied in UV-vis measurements. The absorption peak at 350 nm gradually disappears when the pH is lowered from 5.8 to 2.8 and reappears again when the pH is increased. Based on literature, we expect this absorption to be the $OH^- \rightarrow$ Cu(II) LMCT.[60] We ascribe this change to the protonation of the hydroxide and the reversible formation of a **$[Cu_2L(H_2O)]^{4+}$** complex (See **Figure S18**).

To further gain insight into the Cu^{II}-OH-Cu^{II} motive, we studied how the μ-hydroxyl ligand can form. To do so, the Cu^I complex **$[Cu_2L](OTf)_2$** was synthesized from treatment of **BPMAN** (L) with 1 equivalent of $[CuOTf]_2$·toluene in DCM in 97% yield with NMR data agreeing with reported literature values (See Supporting Information).[42] To see whether the bridging hydroxyl ligand can form, a solution of **$[Cu_2L]^{2+}$** in DCM was exposed to air. This resulted in conversion towards a new, green colored species, which gives rise a set of paramagnetic resonances in the ^{1}H-NMR spectrum that match the resonances found for **$[Cu_2L(\mu\text{-}OH)]^{3+}$** (Spec. Yield= 29%, see Supporting Information section 7.1). Interestingly, within two minutes of exposing the DCM solution to air a short-lived (only trace amounts detectable after 1h)

intermediate was observed in the ^{1}H-NMR spectrum. This could be one of the dicopper(II) species along the possible sequence of the peroxo,[42] hydroperoxo, and oxo intermediates leading up to the formation of **$[Cu_2L(\mu\text{-}OH)]^{3+}$**. Dicopper(II) μ-O species are highly basic[61] and are capable of abstracting a proton from introduced moisture, the solvent or one of the benzylic positions of the ligand. The abstraction of a proton from the benzylic positions of the BPMAN ligand is also in line with the low spectroscopic yield of 29% found for this reaction and the progressive color change of the mixture to dark orange overnight. To probe this hypothesis further, a DCM solution of **$[Cu_2L]^{2+}$** was treated anaerobically with 1 equivalent of the oxo transfer agent iodosylbenzene (PhIO) which resulted in the formation of a progressively darker orange reaction mixture. Analysis of the ^{1}H-NMR spectrum of this mixture revealed **$[Cu_2L(\mu\text{-}OH)]^{3+}$** as the only observable species in a spectroscopic yield of 14% (See Supporting Information section 7.2).

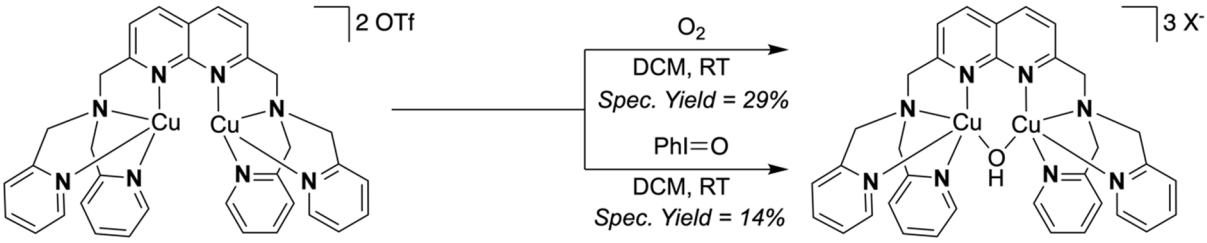

Figure 5 Overview of the reactions taking place when a solution of the **$[Cu_2L](OTf)_2$** complex in DCM is exposed to air or to PhIO, resulting in the formation of the oxidized **$[Cu_2L(\mu\text{-}OH)]^{3+}$** cation in low spectroscopic yields.

Next, the aptitude of the reduced **$[Cu_2L](OTf)_2$** complex to form the Cu^{II}-OH-Cu^{II} motive was confirmed in electrochemical experiments as well. The redox couple of **$[Cu_2L]^{2+}$**, lacking the μ-hydroxyl ligand, was recorded in acetonitrile solution under inert conditions (**Figure 6b**). From these measurements it is evident that the reduction and oxidation peak of **$[Cu_2L]^{2+}$** shifted to more positive potentials compared to the Cu^{II}-OH-Cu^{II} species. This is an indication that the oxidized **$[Cu_2L]^{4+}$** complex can be formed in acetonitrile. Moreover, this again suggests that the negatively charged μ-hydroxyl ligand stabilizes the oxidized dinuclear copper core in **$[Cu_2L(\mu\text{-}OH)]^{3+}$** and that there is a thermodynamic driving force to form this ligand (**Figure 6b-c**).

In the same experiment in water, it is possible for OH^- to bind to the dicopper core when **$[Cu_2L]^{2+}$** is oxidized and **$[Cu_2L(\mu\text{-}OH)]^{3+}$** instead of **$[Cu_2L]^{4+}$** forms (See **Figure S28**). Interestingly, exposure of the **$[Cu_2L]^{2+}$** acetonitrile solution to oxygen from the air will form the **$[Cu_2L(\mu\text{-}OH)]^{3+}$** species only when a proton source is added, while the complex seems to undergo decomposition to unidentified species when no source of protons is available (See Supporting Information section 8). It is to be expected that this decomposition is caused by the abstraction of a proton from the ligand, which agrees with the observed reactivity described in the previous section. In this way, the reactivity studies and

electrochemical experiments show good agreement, and together highlight the fast formation of the μ-hydroxyl ligand if the complex is in the presence of both an oxygen and a proton source.

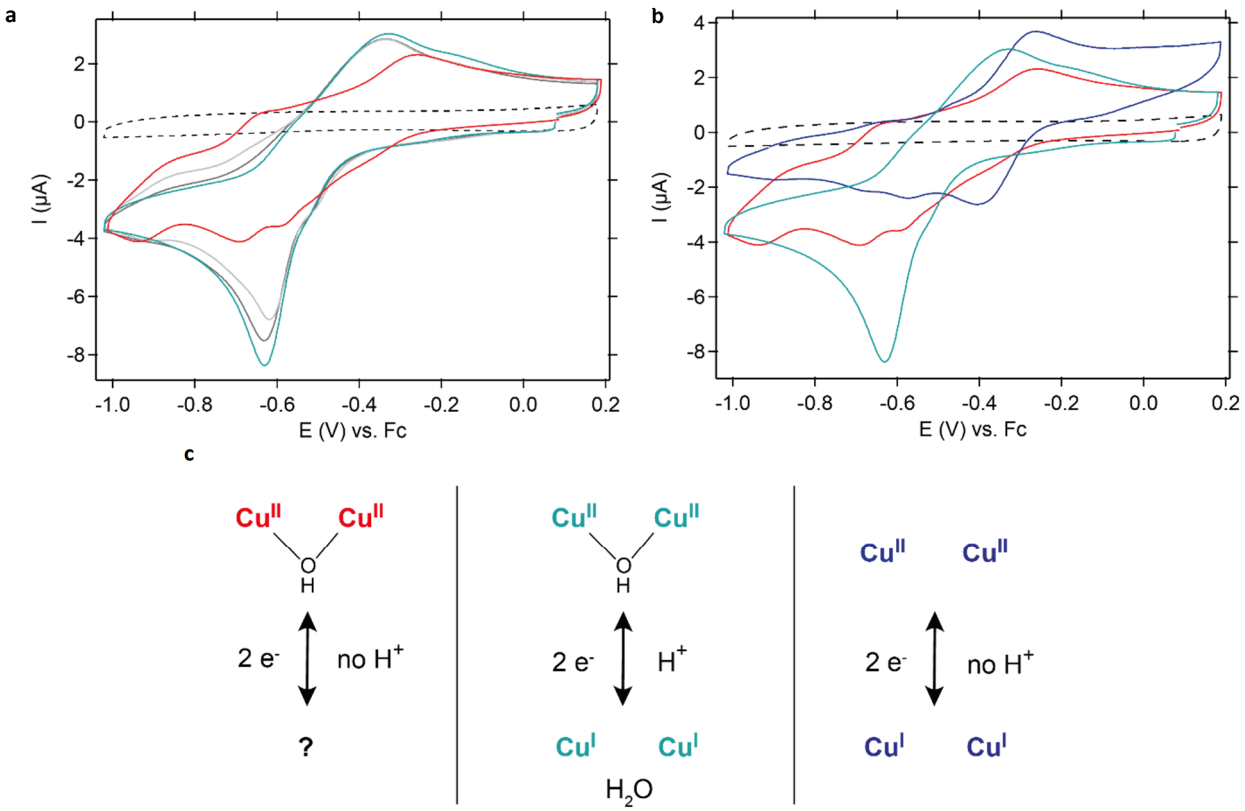

Figure 6 a) CVs of 0.3 mM **$[Cu_2L(\mu\text{-}OH)]^{3+}$** with no (red), 0.15 mM (light grey), 0.6 mM (dark grey), and 1.0 mM (light blue) $TEAPF_6$ present. **b)** CVs of 0.3 mM **$[Cu_2L(\mu\text{-}OH)]^{3+}$** with (light blue) and without (red) 1.0 mM $TEAPF_6$ compared to the 0.3 mM **$[Cu_2L]^{2+}$** redox couple (dark blue). **c)** Schematic overview of the redox processes taking place in figure **b)**. Conditions: 0.1 M $TBAPF_6$ in MeCN, Ar atmosphere, 293 K, 100 mV/s scan rate.

Reaction kinetics of the ORR and HPRR

To get insight into the catalytic mechanism that follows upon reduction of **$[Cu_2L(\mu\text{-}OH)]^{3+}$**, catalyst concentration dependencies were determined for the ORR and HPRR (**Figure 7a-b**). These dependencies were studied in the regime of low catalyst concentrations (1-4 μM), as this will not result in substrate-limited conditions. Additionally, the H_2O_2 concentration was varied to determine the reaction dependency in substrate (**Figure 7c-d**). Since a clear catalytic plateau was absent, the dependence in H_2O_2 concentration was determined at a potential of 0.2 V vs. RHE. In both the ORR and HPRR a linear first-order dependence of the catalytic current on the catalyst concentration was observed. In addition, a first-order dependence of the catalytic current on the substrate concentration for the HPRR was observed. This first-order dependence in both catalyst and substrate concentration indicates that during catalysis of the HPRR one molecule of H_2O_2 reacts at the dinuclear copper core of a single catalyst molecule. For the ORR the substrate dependence was not determined, although we

assume that in the same manner only one molecule of oxygen at a time will react at the dinuclear copper site.

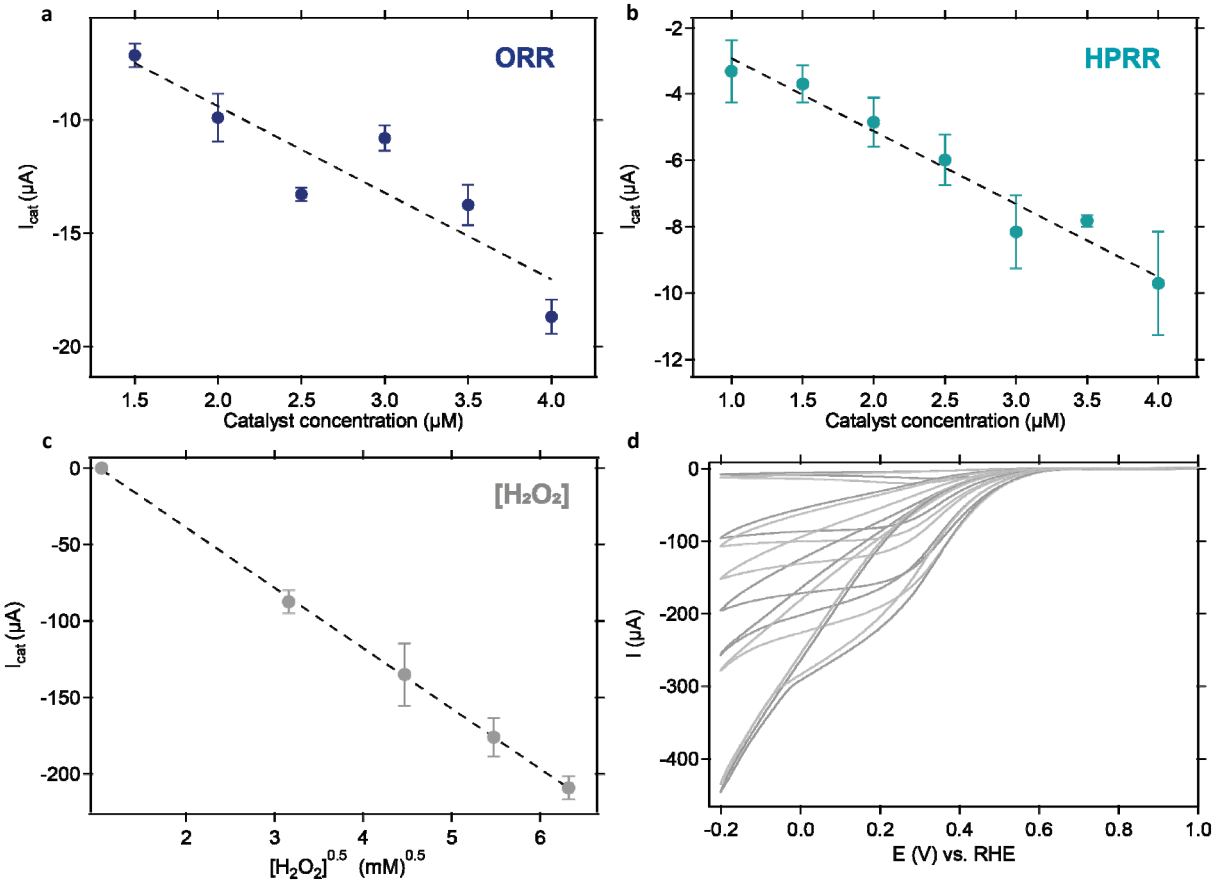

Figure 7 The background-corrected catalytic currents plotted against the **a)** catalyst concentration for the ORR, **b)** catalyst concentration for the HPRR (1.1 mM H_2O_2), **c)** square root of the H_2O_2 concentration for the HPRR at 0.2 V vs. RHE (0.15 mM **$[Cu_2L(\mu\text{-}OH)]^{3+}$**) and **d)** the CVs of the HPRR corresponding to figure c. In figure a-c, the data points are the average of two measurements. Conditions: 0.1 M PB pH 7, Ar or O_2 atmosphere, 293 K, 100 mV/s scan rate

Next, the same experiments were used to gain insight into the reaction kinetics. For low concentrations of **$[Cu_2L(\mu\text{-}OH)]^{3+}$**, the reaction is not limited by substrate availability and a quantitative value for the observed rate constant (k_{obs}) can be determined from the catalytic current enhancement method using **Equation 1**.[62]

$$\frac{i_{cat}}{i_p} = 2.24n\sqrt{\frac{RT}{Fv}k_{obs}} \qquad \textbf{(1)}$$

Where i_{cat} is the measured catalytic current, i_p is the peak current in absence of substrate, n is the number of electrons transferred in the catalytic reaction, T is the temperature (T = 293 K), v is the scan rate (v = 100 mV/s) and k_{obs} is the observed first-order rate constant. The theoretical i_p was calculated from the Randles-Sevcik equation, because of the low catalyst concentrations (See Supporting Information section 5). It is not possible to determine the number of electrons transferred in the ORR

from stationary CV experiments, hence we determined the k_{obs} for the ORR as the range between the minimum number of electrons transferred to reduce oxygen to H_2O_2 (n=2) and the complete reduction of oxygen to water (n=4). The calculated values for k_{obs} from the current enhancement method lie between $3.7 \pm 1.0 \times 10^3\ s^{-1}$ and $14.7 \pm 4.2 \times 10^3\ s^{-1}$ for the ORR and is $4.8 \pm 1.4 \times 10^3\ s^{-1}$ for the HPRR (See Supporting Information section 9). Clearly, the values of k_{obs} determined for the ORR and HPRR lie within the same order of magnitude. This could be suggestive of the same rate determining step (RDS) in the ORR and HPRR, which is in contrast with the observed rate constants for Cu(tmpa), which lie two orders of magnitude apart.[63]

Interestingly, determination of the k_{obs} for **$[Cu_2L(\mu\text{-}OH)]^{3+}$** in the same manner in acetate buffer of pH 4.8, resulted in a k_{obs} for the HPRR that is comparable with the value at pH 7, whereas the k_{obs} for the ORR became almost four times as large (See **Table S1**). This observation indicates that the k_{obs} of the ORR is proton dependent. A logical explanation for the larger k_{obs} of the ORR under acidic conditions, is that the RDS involves a protonation step, which suggests that the protonation involved in the reduction of **$[Cu_2L(\mu\text{-}OH)]^{3+}$** is the RDS of the ORR. The fact that the k_{obs} of the HPRR is not influenced by the pH, can be explained by the fact that after reduction of the catalyst, the HPRR mechanism is followed by another slow step that does not lead to a general increase of the observed rate. The observation that the rate of the HPRR is slower than the rate of the ORR is in turn in line with was observed previously for Cu(tmpa).[63]

Further insight into the HPRR mechanism

Intrigued by the proton-independent k_{obs} of the HPRR, we further investigated the reaction mechanism. First, a solvent kinetic isotope effect (KIE) of 1.08 ± 0.25 for the HPRR was determined under non-substrate limiting conditions (See Supporting Information section 10). This value indicates either the absence of a KIE, or the presence of a minor secondary KIE, suggesting that the RDS of the reaction indeed does not involve breaking of an O-H bond. Such a small KIE is in contrast with the previously determined KIE of Cu(tmpa) for the HPRR of 1.4-1.7, which was proposed to go through a Fenton-type mechanism, producing radical species upon homolytical cleavage of the O-O bond.[63] To exclude such a Fenton-type mechanism for **$[Cu_2L(\mu\text{-}OH)]^{3+}$**, hydroxyl radical trapping experiments for the HPRR were carried out during which no radicals could be detected (See Supporting Information section 11).

Interestingly, exposing a degassed D_2O suspension of **$[Cu_2L]^{2+}$** to an equivalent of H_2O_2 led to the instant formation of a green, water-soluble species that gave rise to a different paramagnetic ^{1}H-NMR spectrum than found for **$[Cu_2L(\mu\text{-}OH)]^{3+}$** (See Supporting Information section 7.3). Additionally, two absorption bands arose in the UV-Vis spectrum at 620 and 660 nm after the reaction with H_2O_2 (See

Figure S24). These two observations suggest that oxidation of the Cu centers to Cu(II) has occurred. The difference in NMR spectra raised the question as to what might be bound to the copper centers. The oxidation of the Cu centers pointed towards cleavage of the O-O bond of H_2O_2 and hinted at the fact that the species being formed might be the **$[Cu_2L(\mu\text{-}OH)_2]^{2+}$** species we postulated to form at high pH regimes in the Pourbaix diagram. To investigate this, we exposed a **$[Cu_2L(\mu\text{-}OH)]^{3+}$** solution in D_2O to an equivalent of KOH (See Supporting Information section 7.4). This indeed gave rise to the same resonances in the paramagnetic ^{1}H-NMR spectrum as found for the reaction between **$[Cu_2L]^{2+}$** and H_2O_2. Considering the reactants in the two separate reactions and the measurements on the Pourbaix diagram that indicate that under basic conditions such a species can form, led us to confirm this new species as **$[Cu_2L(\mu\text{-}OH)_2]^{2+}$**. The limited stability of this bis-hydroxide upon removal of the aqueous solvent however prohibited further characterization of this species. The instability of the **$[Cu_2L(\mu\text{-}OH)_2]^{2+}$** species suggest that under non-basic conditions one of the μ-OH ligands is readily protonated to produce **$[Cu_2L(\mu\text{-}OH)]^{3+}$** and H_2O.

Combining the experiments on the HPRR, strong evidence is found for metal-metal cooperativity being involved in the catalytic mechanism. Firstly, there is a first order dependence of the catalytic rate on the concentration of catalyst and the concentration of H_2O_2. This validates that a single molecule of H_2O_2 will be reduced at the dicopper core of the catalyst. Another observation is the fact that **$[Cu_2L(\mu\text{-}OH)_2]^{2+}$** is formed when **$[Cu_2L]^{2+}$** is reacted with H_2O_2. Such a species can only form if the O-O bond is cleaved after binding of H_2O_2 between both copper cores. In addition, **$[Cu_2L(\mu\text{-}OH)]^{3+}$** catalyzes the HPRR via a different pathway than the mononuclear Cu(tmpa) complex.[63] Whereas for Cu(tmpa) a significant KIE is observed and the mechanism is proposed to go through a Fenton-type mechanism, our experiments on **$[Cu_2L(\mu\text{-}OH)]^{3+}$** exclude such a pathway. It is therefore most likely that **$[Cu_2L(\mu\text{-}OH)]^{3+}$** binds H_2O_2 via a different binding motif involving interactions with both copper centers, instead of end-on binding as was proposed for Cu(tmpa).[63]

The selectivity of the ORR

After gaining insights into HPRR mechanism and having a strong indication that both copper centers cooperate in the binding of the H_2O_2 and cleavage of the O-O bond, we set out to investigate the mechanism and cooperativity in the ORR. As stated before, H_2O_2 is found as a detectable intermediate in the electrochemical ORR mechanism of other copper complexes with tetradentate pyridylamine ligands.[36, 39, 41, 53, 54] Hence, it is interesting to see whether the HPRR is part of the ORR occurring via two sequential 2-electron reductions, or whether **$[Cu_2L(\mu\text{-}OH)]^{3+}$** can directly reduce oxygen to water via a 4-electron pathway, similar to MCOs. Therefore, rotating (ring) disk electrode (R(R)DE) experiments were employed.

First, it is important to realize that in the same manner as in stationary CV experiments, the homogeneous catalytic activity of **$[Cu_2L(\mu\text{-}OH)]^{3+}$** in RRDE experiments was ensured by investigating the formation of any active deposits (See Supporting Information section 12.3). Upon recording a CV in a solution of **$[Cu_2L(\mu\text{-}OH)]^{3+}$**, and subsequently recording a CV of the same electrode in a blank solution that does not contain any catalyst, it was shown that a catalytically active, heterogeneous deposit forms on the electrode during the ORR. Under RRDE conditions, this deposit is less active than the homogeneous catalyst in solution (See **Figure S39a**). Next, the selectivity for the 4 or 2 electron ORR of the catalyst in solution and the formed deposits were compared, and it was shown that these experiments have a comparable outcome (See **Figure S39b**). This verifies that the formed deposits do not affect the observed selectivity of **$[Cu_2L(\mu\text{-}OH)]^{3+}$**. To ensure that we exclusively study the homogeneous catalyst in solution, only the first scan of any RRDE experiment is used to assign the catalytic activity and selectivity of **$[Cu_2L(\mu\text{-}OH)]^{3+}$**. In chronoamperometry measurements (CA) it is not possible to exclude contribution of any deposited species that form during the experiment. However, we do not observe any change in selectivity or activity over the course of CA experiment indicating that no build-up of a catalytically competent species occurs. An exception is when a potential close to the onset of 0.4 V vs. RHE is applied. In this case, we observe a change in the selectivity over time, which we attribute to the fact that under these conditions the current is low in general, which will easily lead to deviations in the selectivity (See **Figure S38**).

RDE CVs of **$[Cu_2L(\mu\text{-}OH)]^{3+}$** recorded in PB of pH 7 at various rotation rates show slow catalysis of the ORR, because even at a low potential of −0.4 V vs. RHE no clear mass-transport limited plateau is reached (See **Figure S35**). More interestingly, RRDE measurements of **$[Cu_2L(\mu\text{-}OH)]^{3+}$** were carried out to determine the selectivity of the ORR over the full potential window. In RRDE measurements the hydrogen peroxide that is produced at the GC disk can be quantified by oxidation at the Pt ring (See Supporting Information section 12.2). **Figure 8** shows that **$[Cu_2L(\mu\text{-}OH)]^{3+}$** selectively catalyzes the four-electron ORR in both linear sweep voltammetry (LSV) and CA measurements, producing more than 70% H_2O over the main part of the potential window. Only close to the onset potential in the LSV the selectivity to H_2O_2 is high, which is likely to be less accurate as the currents are (too) low. To exclude that any H_2O_2 is decomposed by the catalyst before it can be detected at the ring, the stability of H_2O_2 solutions in the presence of **$[Cu_2L(\mu\text{-}OH)]^{3+}$** was studied. These experiments confirm that the catalyst is not capable of breaking down H_2O_2 before it reaches the ring (See Supporting Information section 13).

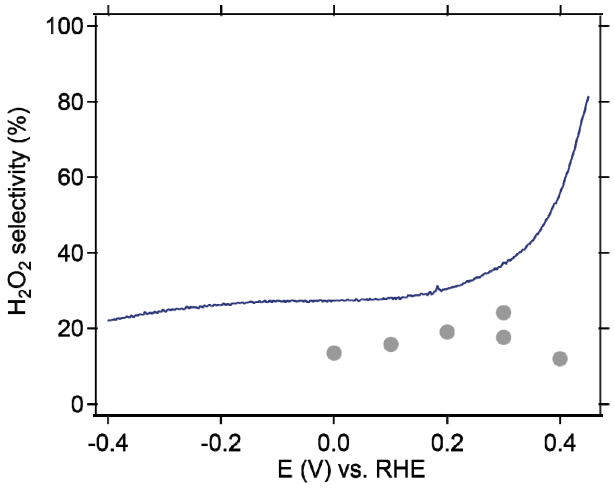

Figure 8 H_2O_2 selectivity in the ORR as determined from RRDE LSV measurements (dark blue line) and CA measurements (grey dots) at different potentials. The LSV currents were corrected for the currents measured between 0.8 - 1.0 V vs. RHE and the CA points were corrected for the currents measured at 0.8 V vs. RHE preceding the experiment. Conditions: 0.15 mM **$[Cu_2L(\mu\text{-}OH)]^{3+}$**, O_2 atmosphere, 0.1 M PB pH 7, 293 K, 1600 RPM, Pt ring at 1.2 V vs. RHE.

It is likely that the preference of **$[Cu_2L(\mu\text{-}OH)]^{3+}$** to catalyze the ORR in a four-electron process arises from metal-metal cooperativity in the dinuclear copper core. In **$[Cu_2L(\mu\text{-}OH)]^{3+}$** the naphthyridine-based ligand enforces the two copper atoms to bind in close proximity and in this way facilitates bridging binding modes for exogeneous ligands, like the peroxo intermediate.[42] This is in contrast with mononuclear copper complexes, that can either bind a (hydro)peroxo ligand in an end-on manner or upon reaction with oxygen will slowly dimerize to form a peroxo dicopper complex,[27] as is observed for Cu(tmpa).[64] The ORR selectivity to water of 70% by **$[Cu_2L(\mu\text{-}OH)]^{3+}$** stands out compared to the selectivity of Cu(tmpa), which only converts 20% of oxygen to water in the presence of high concentrations of oxygen.[41] The improved selectivity of **$[Cu_2L(\mu\text{-}OH)]^{3+}$** points to a different mechanism in which the enforced bridging geometries result in the thermodynamic stabilization of the formed (hydro)peroxo intermediates and facilitate the easy cleavage of the O-O bond. Furthermore, we hypothesize that the energy barrier to release any intermediate ORR products like H_2O_2 from the dinuclear copper core is high. On one hand the release of H_2O_2 is disfavored kinetically due to the proximal oxygen being not easily accessible for protonation. On the other hand, liberating any of the (hydro)(per)oxo ligands results in the formation of the bare dinuclear Cu^{II} Cu^{II} core, which is energetically disfavored due to severe electrostatic repulsions of the two copper centers confined in the rigid naphthyridine framework. Combined, we believe that these are the main arguments that steer the reaction to the four-electron pathway and explain the significant difference in selectivity compared to mononuclear analogues.

Discussion of the ORR mechanisms by $[Cu_2L(\mu\text{-}OH)]^{3+}$ and MCOs

Combining the investigations of the ORR and HPRR, a mechanism for these reactions catalyzed by **$[Cu_2L(\mu\text{-}OH)]^{3+}$** could be established (see **Figure 9**). Starting the catalytic cycle, **$[Cu_2L(\mu\text{-}OH)]^{3+}$** needs to be reduced and the bridging ligand has to dissociate from the dicopper core. Measurements have shown that below pH 7 this process takes place via a PCET step, in which two electrons and one proton are transferred and the hydroxide is released as H_2O. Between pH 7 and 9 insufficient protons are available and the bridging ligand is released as is. Above pH 9, a **$[Cu_2L(\mu\text{-}OH)_2]^{2+}$** species forms that is reduced in a two electron and one proton PCET process. In addition, CV measurements have shown that the presence of the μ-OH moiety stabilizes the Cu^{II}-OH-Cu^{II} core, which makes activation of the catalyst harder and slows down the electron transfer in general. In line with this observation, the determined k_{obs} values for both HPRR and ORR at pH 7 lie within the same order of magnitude, suggesting that in both reactions the reduction of **$[Cu_2L(\mu\text{-}OH)]^{3+}$** and release of OH^- is the rate-determining step.

After reduction and release of the bridging ligand, oxygen can bind to the Cu^I Cu^I core. From a previous study by Lippard and co-workers on the same compound, it is known that the μ-1,2-peroxo species can be formed,[42] hence it is likely that the same species will be formed here. Next, we hypothesize that proton transfer will lead to the formation of a hydroperoxo species. RRDE experiments show that small quantities of H_2O_2 are produced during the ORR. It is speculated that the hydroperoxo can bind in a μ-1,1 manner as such μ-1,1-hydroperoxo species have been shown to be able to form previously.[31, 65-68] From this intermediate small quantities of H_2O_2 can be formed upon protonation. Likewise, it is anticipated that the high selectivity of **$[Cu_2L(\mu\text{-}OH)]^{3+}$** compared to the mononuclear Cu(tmpa) complex for the four-electron ORR arises from the stabilization of this μ-1,1-hydroperoxo species between both copper atoms. In this way, the four-electron ORR will take place via protonation of the distal oxygen atom and prevents formation of the disfavored bare Cu^{II}-Cu^{II} species. In the next step, two electrons and two protons are transferred. This leads to cleavage of the O-O bond, and generation of H_2O. Whether this step proceeds directly or via the intermediate production of a μ-oxo species cannot be addressed experimentally. We have shown however through our studies with the oxo-transfer agent PhIO that if such a oxo-species would form it would readily be protonated, reforming **$[Cu_2L(\mu\text{-}OH)]^{3+}$**.

Next to the ORR mechanism, the off-cycle HPRR mechanism was studied. After reduction of **$[Cu_2L(\mu\text{-}OH)]^{3+}$**, H_2O_2 binds to the dicopper core, upon which two electrons are transferred to break the O-O bond and the **$[Cu_2L(\mu\text{-}OH)_2]^{2+}$** species is formed. Due to the relative instability of this bis-μ-OH species, we hypothesize that this species will be quickly protonated to regenerate the stable **$[Cu_2L(\mu\text{-}OH)]^{3+}$** complex. Though this HPRR mechanism is not part of the ORR, this reaction as well shows how having two copper centers in close proximity allows for the cooperative activation of substrates.

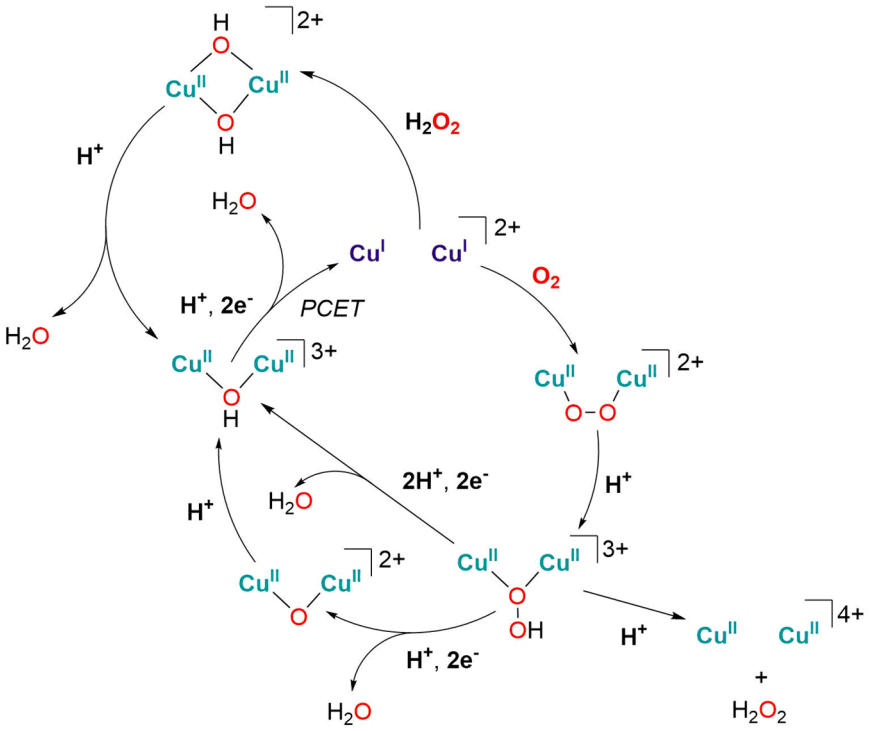

Figure 9 Proposed stepwise mechanism for the ORR and HPRR by $[Cu_2L(\mu\text{-}OH)]^{3+}$. For clarity the BPMAN ligand is not depicted. PCET step takes place below pH 7.

Next, we can identify how the ORR mechanism of **$[Cu_2L(\mu\text{-}OH)_2]^{3+}$** relates to that of MCOs. In both the synthesized **$[Cu_2L(\mu\text{-}OH)]^{3+}$** complex and T3 site of the MCO resting state a μ-OH ligand is present.[12] From our study it is apparent that the formation of the Cu-OH-Cu motif is a severe thermodynamic driving force, hence the presence of the bridging hydroxyl ligand can be linked to slow electron transfer kinetics and a large energy barrier to activate the catalyst. This is comparable to what is observed for MCOs, where the presence of the μ-OH makes reduction of the RO state too slow to be part of the catalytic cycle.[22] In addition, the presence of the Cu-OH-Cu motif makes that reduction of **$[Cu_2L(\mu\text{-}OH)]^{3+}$**, below pH 7, and reduction of the T3 site in the RO state take place in a similar PCET mechanism, in which two electrons and a proton are transferred to protonate the μ-OH and release H_2O.

In the next step of the catalytic cycle, an oxygen molecule can bind to the FR state of MCOs resulting in the formation of a μ_3-1,1,2-peroxo intermediate in an irreversible manner.[17] When **$[Cu_2L]^{2+}$** reacts with oxygen, it is likely that a μ-1,2-peroxo binds between both coppers, as observed previously.[42] In MCOs, the binding mode of the μ_3-1,1,2 peroxide is essential for the cleavage of the O-O bond and the four-electron reduction of oxygen.[17] Compared to MCOs, **$[Cu_2L(\mu\text{-}OH)]^{3+}$** binds this (hydro)peroxo differently, but we attribute the greatly improved selectivity towards the four-electron ORR (compared to the selectivity of mononuclear Cu-tmpa towards two-electron ORR) to the ability to bind catalytic intermediates in a bridging manner. The fact that **$[Cu_2L(\mu\text{-}OH)]^{3+}$** still generates small amounts of H_2O_2 during the ORR may be explained by the hypothesis that the dicopper core in the catalyst will bind the

(hydro)peroxo intermediates less tightly than the three copper atoms in the TNC, hence it will be easier to protonate these intermediates and liberate low amounts of H_2O_2 from the catalyst.

To complete the catalytic ORR cycle in MCOs, the NI state containing a μ_3-O and μ-OH is formed from the PI state after the second two-electron step and cleavage of the O-O bond.[16] Next, the FR state is regenerated rapidly by protonation and reduction of this highly basic μ_3-O ligand.[21] In **$[Cu_2L(\mu\text{-}OH)]^{3+}$**, a μ_3-oxo cannot form, instead we hypothesize that **$[Cu_2L(\mu\text{-}OH)]^{3+}$** is regenerated upon the two electron reduction of the hydroperoxo intermediate, either directly or through a μ-O intermediate. Whereas in most MCOs the NI intermediate is easily reduced to the FR intermediate for subsequent turnovers, re-reduction of **$[Cu_2L(\mu\text{-}OH)]^{3+}$** is less facile for the abovementioned reasons. Interestingly, in metallooxidases, a less-studied class of MCOs, the NI might rapidly decay to the RO state of the enzyme, which results in slow turnovers and the internal electron transfer to the RO state of the resting enzyme to become rate-limiting.[69] In line with this, we showed for **$[Cu_2L(\mu\text{-}OH)]^{3+}$** that the Cu-OH-Cu motif is formed at the end of the catalytic cycle and reduction of the catalyst is the rate-determining step. Therefore, the catalytic cycle found for **$[Cu_2L(\mu\text{-}OH)]^{3+}$** is more reminiscent of the slow cycle observed in these MCOs.

Conclusion

To conclude, by combining electrochemical measurements and reactivity studies, insights into the mechanisms of the ORR and HPRR catalyzed by **$[Cu_2L(\mu\text{-}OH)]^{3+}$** have been obtained. Some of the key active species along these catalytic pathways were identified, resulting in a detailed understanding of the activity and selectivity of this catalyst. From our study it is evident that metal-metal cooperativity during both HPRR and ORR could be established by the 1,8-naphthyridine backbone that forces both copper atoms in **$[Cu_2L(\mu\text{-}OH)]^{3+}$** closely together. Until now, no other studies on biomimetic copper complexes have given such direct evidence for cooperativity during electrocatalysis of the ORR or HPRR. Following from this, the dinuclear **$[Cu_2L(\mu\text{-}OH)]^{3+}$** complex catalyzes the HPPR and ORR in a different manner than its mononuclear analogue Cu(tmpa).[41, 63] The (hydro)peroxo intermediates that form during the HPRR and ORR are stabilized between both copper centers, and as a result the selectivity for the four-electron reduction of oxygen is greatly improved. While the T3 site in MCOs is not able to bind or reduce oxygen in the absence of the T2 site, the rigid ligand framework in the T3 site-inspired **$[Cu_2L(\mu\text{-}OH)]^{3+}$** complex makes reduction of oxygen possible in absence of a third copper atom. Compared to the ORR mechanism found in MCOs, the reduction of the Cu-OH-Cu motif in **$[Cu_2L(\mu\text{-}OH)]^{3+}$** follows a similar PCET pathway. As a third copper center is absent, the dinuclear copper core in **$[Cu_2L(\mu\text{-}OH)]^{3+}$** will bind the intermediates along the ORR pathway in a different manner than the trinuclear cluster in MCOs. This results in a catalytic pathway that better compares to the slow ORR

cycle in MCOs. Taken together, this work explains how confining the T3-inspired dicopper core in a rigid scaffold at close proximity allows the ORR to take place, in line with what was proposed in literature based on computations. Lastly, this work contributes to better understanding of how the excellent activity and selectivity of MCOs are established, which ultimately can be used for the development of sustainable ORR catalysts.

Acknowledgments

Leonardo Passerini from Leiden University is kindly acknowledged for his help with EPR measurements. Funding was provided by the European Research Council (ERC Proof of Concept grant 899535 Cu4Peroxide to D. G. H. H.) and the Netherlands Organization for Scientific Research (VI.Veni.192.074 to D.L.J.B.).

References

1. Shao, M.; Chang, Q.; Dodelet, J. P.; Chenitz, R., Recent Advances in Electrocatalysts for Oxygen Reduction Reaction. *Chem. Rev.* **2016,** *116* (6), 3594-657.
2. Kulkarni, A.; Siahrostami, S.; Patel, A.; Norskov, J. K., Understanding Catalytic Activity Trends in the Oxygen Reduction Reaction. *Chem. Rev.* **2018,** *118* (5), 2302-2312.
3. Stephens, I. E. L.; Rossmeisl, J.; Chorkendorff, I., Toward sustainable fuel cells. *Science* **2016,** *354* (6318), 1378-1379.
4. Gasteiger, H. A.; Kocha, S. S.; Sompalli, B.; Wagner, F. T., Activity benchmarks and requirements for Pt, Pt-alloy, and non-Pt oxygen reduction catalysts for PEMFCs. *Applied Catalysis B: Environmental* **2005,** *56* (1-2), 9-35.
5. Zaman, S.; Huang, L.; Douka, A. I.; Yang, H.; You, B.; Xia, B. Y., Oxygen Reduction Electrocatalysts toward Practical Fuel Cells: Progress and Perspectives. *Angew. Chem. Int. Ed.* **2021,** *60* (33), 17832-17852.
6. Solomon, E. I.; Sundaram, U. M.; Machonkin, T. E., Multicopper Oxidases and Oxygenases. *Chem. Rev.* **1996,** *96* (7), 2563-2605.
7. Mano, N.; Soukharev, V.; Heller, A., A Laccase-Wiring Redox Hydrogel for Efficient Catalysis of O2 Electroreduction. *J. Phys. Chem. B* **2006,** *110* 11180-11187.
8. Soukharev, V.; Mano, N.; Heller, A., A Four-Electron O2-Electroreduction Biocatalyst Superior to Platinum and a Biofuel Cell Operating at 0.88 V. *J. Am. Chem. Soc.* **2004,** *126*, 8368-8369.
9. Thorum, M. S.; Anderson, C. A.; Hatch, J. J.; Campbell, A. S.; Marshall, N. M.; Zimmerman, S. C.; Lu, Y.; Gewirth, A. A., Direct, Electrocatalytic Oxygen Reduction by Laccase on Anthracene-2-methanethiol Modified Gold. *J Phys Chem Lett* **2010,** *1* (15), 2251-2254.
10. Cole, J. L.; Clark, P. A.; Solomon, E. I., Spectroscopic and Chemical Studies of the Lacease Trinuclear Copper Active Site: Geometric and Electronic Structure. *J Am Chem Soc* **1990,** *112*, 9534-9548.
11. Jones, S. M.; Solomon, E. I., Electron transfer and reaction mechanism of laccases. *Cell Mol Life Sci* **2015,** *72* (5), 869-883.
12. Solomon, E. I.; Heppner, D. E.; Johnston, E. M.; Ginsbach, J. W.; Cirera, J.; Qayyum, M.; Kieber-Emmons, M. T.; Kjaergaard, C. H.; Hadt, R. G.; Tian, L., Copper active sites in biology. *Chem. Rev.* **2014,** *114* (7), 3659-3853.
13. Solomon, E. I.; Augustine, A. J.; Yoon, J., O2 Reduction to H2O by the multicopper oxidases. *Dalton Trans* **2008,** *30*, 3921–3932.
14. Cole, J. L.; Ballou, D. P.; Solomon, E. I., Spectroscopic Characterization of the Peroxide Intermediate in the Reduction of Dioxygen Catalyzed by the Multicopper Oxidases. *J. Am. Chem. Soc.* **1991,** *113* (22), 8544-8546.
15. Shin, W.; Sundaram, U. M.; Cole, J. L.; Zhang, H. H.; Hedman, B.; Hodgson, K. O.; Solomon, E. I., Chemical and Spectroscopic Definition of the Peroxide-Level Intermediate in the Multicopper Oxidases: Relevance to the Catalytic Mechanism of Dioxygen Reduction to Water. *J. Am. Chem. Soc.* **1996,** *118*, 3202-3215.

16. Palmer, A. E.; Lee, S. K.; Solomon, E. I., Decay of the Peroxide Intermediate in Laccase: Reductive Cleavage of the O-O Bond. *J. Am. Chem. Soc.* **2001,** *123*, 6591-6599.
17. Yoon, J.; Solomon, E. I., Electronic structure of the peroxy intermediate and its correlation to the native intermediate in the multicopper oxidases: insights into the reductive cleavage of the O-O bond. *J. Am. Chem. Soc.* **2007,** *129* (43), 13127-13136.
18. Yoon, J.; Solomon, E. I., Electronic structures of exchange coupled trigonal trimeric Cu(II) complexes: Spin frustration, antisymmetric exchange, pseudo-A terms, and their relation to O2 activation in the multicopper oxidases. *Coordination Chemistry Reviews* **2007,** *251* (3-4), 379-400.
19. Lee, S.-K.; DeBeer George, S.; Antholine, W. E.; Hedman, B.; Hodgson, K. O.; Solomon, E. I., Nature of the Intermediate Formed in the Reduction of O2 to H2O at the Trinuclear Copper Cluster Active Site in Native Laccase. *J. Am. Chem. Soc.* **2002,** *124*, 6180-6193.
20. Heppner, D. E.; Kjaergaard, C. H.; Solomon, E. I., Mechanism of the reduction of the native intermediate in the multicopper oxidases: insights into rapid intramolecular electron transfer in turnover. *J. Am. Chem. Soc.* **2014,** *136* (51), 17788-17801.
21. Heppner, D. E.; Kjaergaard, C. H.; Solomon, E. I., Molecular origin of rapid versus slow intramolecular electron transfer in the catalytic cycle of the multicopper oxidases. *J. Am. Chem. Soc.* **2013,** *135* (33), 12212-12215.
22. Yoon, J.; Liboiron, B. D.; Sarangi, R.; Hodgson, K. O.; Hedman, B.; Solomon, E. I., The two oxidized forms of the trinuclear Cu cluster in the multicopper oxidases and mechanism for the decay of the native intermediate. *PNAS* **2007,** *104* (34), 13609-13614.
23. LuBien, C. D.; Winkler, E.; Thamann, T. J.; Scott, R. A.; Co, M. S.; Hodgson, K. O.; Solomon, E. I., Chemical and Spectroscopic Properties of the Binuclear Copper Active Site in Rhus Lacease: Direct Confirmation of a Reduced Binuclear Type 3 Copper Site in Type 2 Depleted Lacease and Intramolecular Coupling of the Type 3 to the Type 1 and Type 2 Copper Sites. *J. Am. Chem. Soc.* **1981,** *103*, 7014-7016.
24. Kau, L.-S.; Spira-Solomon, D. J.; Penner-Hahn, J. E.; Hodgson, K. O.; Solomon, E. I., X-ray Absorption Edge Determination of the Oxidation State and Coordination Number of Copper: Application to the Type 3 Site in Rhus vernicifera Lacease and Its Reaction with Oxygen. *J. Am. Chem. Soc.* **1987,** *109*, 6433-6442.
25. Solomon, E. I.; Chen, P.; Metz, M.; Lee, S.-K.; Palmer, A. E., Oxygen Binding, Activation, and Reduction to Water by Copper Proteins *Angew. Chem. Int. Ed.* **2001,** *40*, 4570-4590.
26. Yoon, J.; Fujii, S.; Solomon, E. I., Geometric and electronic structure differences between the type 3 copper sites of the multicopper oxidases and hemocyanin/tyrosinase. *PNAS* **2009,** *106* (16), 6585-6590.
27. Elwell, C. E.; Gagnon, N. L.; Neisen, B. D.; Dhar, D.; Spaeth, A. D.; Yee, G. M.; Tolman, W. B., Copper-Oxygen Complexes Revisited: Structures, Spectroscopy, and Reactivity. *Chem. Rev.* **2017,** *117* (3), 2059-2107.
28. Mirica, L. M.; Ottenwaelder, X.; Stack, T. D. P., Structure and Spectroscopy of Copper−Dioxygen Complexes. *Chem. Rev.* **2004,** *104*, 1013-1045.
29. Serrano-Plana, J.; Garcia-Bosch, I.; Company, A.; Costas, M., Structural and Reactivity Models for Copper Oxygenases: Cooperative Effects and Novel Reactivities. *Acc. Chem. Res.* **2015,** *48* (8), 2397-2406.
30. Zhang, W.; Moore, C. E.; Zhang, S., Multiple Proton-Coupled Electron Transfers at a Tricopper Cluster: Modeling the Reductive Regeneration Process in Multicopper Oxidases. *J. Am. Chem. Soc.* **2022,** *144* (4), 1709-1717.
31. Fukuzumi, S.; Tahsini, L.; Lee, Y.-M.; Ohkubo, K.; Nam, W.; Karlin, K. D., Factors That Control Catalytic Two- versus Four-Electron Reduction of Dioxygen by Copper Complexes. *J. Am. Chem. Soc.* **2012,** *134* (16), 7025-7035.
32. Mangue, J.; Gondre, C.; Pecaut, J.; Duboc, C.; Menage, S.; Torelli, S., Controlled O2 reduction at a mixed-valent (II,I) Cu2S core. *Chem. Commun.* **2020,** *56* (67), 9636-9639.

33. Tahsini, L.; Kotani, H.; Lee, Y. M.; Cho, J.; Nam, W.; Karlin, K. D.; Fukuzumi, S., Electron-transfer Reduction of Dinuclear Copper Peroxo and Bis-mu-oxo Complexes Leading to the Catalytic Four-electron Reduction of Dioxygen to Water. *Chem. Eur. J.* **2012,** *18* (4), 1084-1093.
34. Torelli, S.; Orio, M.; Pecaut, J.; Jamet, H.; Le Pape, L.; Menage, S., A {Cu2S}2+ Mixed-Valent Core Featuring a Cu-Cu Bond. *Angew. Chem.* **2010,** *122*, 8425-8428.
35. Gomila, A.; Le Poul, N.; Kerbaol, J. M.; Cosquer, N.; Triki, S.; Douziech, B.; Conan, F.; Le Mest, Y., Electrochemical behavior and dioxygen reactivity of tripodal dinuclear copper complexes linked by unsaturated rigid spacers. *Dalton Trans.* **2013,** *42* (6), 2238-2253.
36. van Dijk, B.; Kinders, R.; Ferber, T. H.; Hofmann, J. P.; Hetterscheid, D. G. H., A Selective Copper Based Oxygen Reduction Catalyst for the Electrochemical Synthesis of H2O2 at Neutral pH. *ChemElectroChem* **2022,** *9* (3), e202101692.
37. Tse, E. C.; Schilter, D.; Gray, D. L.; Rauchfuss, T. B.; Gewirth, A. A., Multicopper models for the laccase active site: effect of nuclearity on electrocatalytic oxygen reduction. *Inorg. Chem.* **2014,** *53* (16), 8505-8516.
38. van Dijk, B.; Hofmann, J. P.; Hetterscheid, D. G. H., Pinpointing the active species of the Cu(DAT) catalyzed oxygen reduction reaction. *Phys. Chem. Chem. Phys.* **2018,** *20* (29), 19625-19634.
39. Smits, N. W. G.; Rademaker, D.; Konovalov, A. I.; Siegler, M. A.; Hetterscheid, D. G. H., Influence of the spatial distribution of copper sites on the selectivity of the oxygen reduction reaction. *Dalton Trans.* **2022,** *51* (3), 1206-1215.
40. Thiyagarajan, N.; Janmanchi, D.; Tsai, Y. F.; Wanna, W. H.; Ramu, R.; Chan, S. I.; Zen, J. M.; Yu, S. S., A Carbon Electrode Functionalized by a Tricopper Cluster Complex: Overcoming Overpotential and Production of Hydrogen Peroxide in the Oxygen Reduction Reaction. *Angew. Chem. Int. Ed.* **2018,** *57* (14), 3612-3616.
41. Langerman, M.; Hetterscheid, D. G. H., Fast Oxygen Reduction Catalyzed by a Copper(II) Tris(2-pyridylmethyl)amine Complex through a Stepwise Mechanism. *Angew. Chem. Int. Ed.* **2019,** *58* (37), 12974-12978.
42. He, C.; DuBois, J. L.; Hedman, B.; Hodgson, K. O.; Lippard, S. J., A Short Copper Copper Distance in a (mu-1,2-Peroxo)dicopper(II) Complex Having a 1,8-Naphthyridine Unit as an Additional Bridge. *Angew. Chem. Int. Ed.* **2001,** *40* (8), 1484-1487.
43. Su, X. J.; Gao, M.; Jiao, L.; Liao, R. Z.; Siegbahn, P. E.; Cheng, J. P.; Zhang, M. T., Electrocatalytic water oxidation by a dinuclear copper complex in a neutral aqueous solution. *Angew. Chem. Int. Ed.* **2015,** *54* (16), 4909-4914.
44. Bera, J. K.; Sadhukhan, N.; Majumdar, M., 1,8-Naphthyridine Revisited: Applications in Dimetal Chemistry. *Eur. J. Inorg. Chem.* **2009,** *2009* (27), 4023-4038.
45. Desnoyer, A. N.; Nicolay, A.; Rios, P.; Ziegler, M. S.; Tilley, T. D., Bimetallics in a Nutshell: Complexes Supported by Chelating Naphthyridine-Based Ligands. *Acc. Chem. Res.* **2020,** *53* (9), 1944-1956.
46. He, C.; Lippard, S. J., Design and Synthesis of Multidentate Dinucleating Ligands Based on 1,8-Naphthyridine. *Tetrahedron* **2000,** *56*, 8245-8252.
47. He, C.; Barrios, A. M.; Lee, D.; Kuzelka, J.; Davydov, R. M.; Lippard, S. J., Diiron Complexes of 1,8-Naphthyridine-Based Dinucleating Ligands as Models for Hemerythrin. *J. Am. Chem. Soc.* **2000,** *122* (51), 12683-12690.
48. Kuzelka, J.; Mukhopadhyay, S.; Spingler, B.; Lippard, S. J., Modeling Features of the Non-Heme Diiron Cores in O2-Activating Enzymes through the Synthesis, Characterization, and Oxidation of 1,8-Naphthyridine-Based Complexes. *Inorg. Chem.* **2003,** *42* (20), 6447-6457.
49. He, C.; Lippard, S. J., Synthesis and Electrochemical Studies of Diiron Complexes of 1,8-Naphthyridine-Based Dinucleating Ligands to Model Features of the Active Sites of Non-Heme Diiron Enzymes *Inorg. Chem.* **2001,** *40* (7), 1414-1420.
50. He, C.; Lippard, S. J., Synthesis and Characterization of Several Dicopper(I) Complexes and a Spin-Delocalized Dicopper(I,II) Mixed-Valence Complex Using a 1,8-Naphthyridine-Based Dinucleating Ligand *Inorg. Chem.* **2000,** *39* (23), 5225-5231.

51. Biswas, A.; Das, L. K.; Drew, M. G.; Diaz, C.; Ghosh, A., Insertion of a Hydroxido Bridge into a Diphenoxido Dinuclear Copper(II) Complex: Drastic Change of the Magnetic Property from Strong Antiferromagnetic to Ferromagnetic and Enhancement in the Catecholase Activity. *Inorg. Chem.* **2012,** *51* (19), 10111-10121.
52. Bansal, D.; Gupta, R., Hydroxide-bridged dicopper complexes: the influence of secondary coordination sphere on structure and catecholase activity. *Dalton Trans.* **2017,** *46* (14), 4617-4627.
53. Smits, N. W. G.; van Dijk, B.; de Bruin, I.; Groeneveld, S. L. T.; Siegler, M. A.; Hetterscheid, D. G. H., Influence of Ligand Denticity and Flexibility on the Molecular Copper Mediated Oxygen Reduction Reaction. *Inorg Chem* **2020,** *59* (22), 16398-16409.
54. Chowdhury, S. N.; Biswas, S.; Das, P.; Paul, S.; Biswas, A. N., Oxygen Reduction Assisted by the Concert of Redox Activity and Proton Relay in a Cu(II) Complex. *Inorg. Chem.* **2020,** *59* (19), 14012-14022.
55. Hall, S. B.; Khudaisha, E. A.; Hart, A. L., Electrochemical oxidation of hydrogen peroxide at platinum electrodes. Part III: Effect of temperature. *Electrochimica Acta* **1999,** *44*, 2455-2462.
56. van Stroe-Biezen, S. A. M.; Everaerts, F. M.; Janssen, L. J. J.; Tacken, R. A., Diffusion coefficients of oxygen, hydrogen peroxide and glucose in a hydrogel. *Analytica Chimica Acta* **1993,** *273*, 553-560.
57. Lee, K. J.; McCarthy, B. D.; Dempsey, J. L., On decomposition, degradation, and voltammetric deviation: the electrochemist's field guide to identifying precatalyst transformation. *Chem. Soc. Rev.* **2019,** *48* (11), 2927-2945.
58. Macpherson, J. V., A practical guide to using boron doped diamond in electrochemical research. *Phys. Chem. Chem. Phys.* **2015,** *17* (5), 2935-2949.
59. Costentin, C., Electrochemical Approach to the Mechanistic Study of Proton-Coupled Electron Transfer. *Chem. Rev.* **2008,** *108* (7), 2145-2179.
60. Ghosh, D.; Mukherjee, R., Modeling Tyrosinase Monooxygenase Activity. Spectroscopic and Magnetic Investigations of Products Due to Reactions between Copper(I) Complexes of Xylyl-Based Dinucleating Ligands and Dioxygen: Aromatic Ring Hydroxylation and Irreversible Oxidation Products. *Inorg. Chem.* **1998,** *37*, 6597-6605.
61. Haack, P.; Limberg, C., Molecular Cu(II)-O-Cu(II) complexes: still waters run deep. *Angew. Chem. Int. Ed.* **2014,** *53* (17), 4282-4293.
62. Lee, K. J.; Elgrishi, N.; Kandemir, B.; Dempsey, J. L., Electrochemical and spectroscopic methods for evaluating molecular electrocatalysts. *Nature Reviews Chemistry* **2017,** *1* (5), 1-14.
63. Langerman, M.; Hetterscheid, D. G. H., Mechanistic Study of the Activation and the Electrocatalytic Reduction of Hydrogen Peroxide by Cu-tmpa in Neutral Aqueous Solution. *ChemElectroChem* **2021,** *8* (15), 2783-2791.
64. Fukuzumi, S.; Kotani, H.; Lucas, H. R.; Doi, K.; Suenobu, T.; Peterson, R. L.; Karlin, K. D., Mononuclear copper complex-catalyzed four-electron reduction of oxygen. *J. Am. Chem. Soc.* **2010,** *132* (20), 6874-6875.
65. Root, D. E.; Mahroof-Tahir, M.; Karlin, K. D.; Solomon, E. I., Effect of Protonation on Peroxo-Copper Bonding: Spectroscopic and Electronic Structure Study of [Cu2((UN-O-)(OOH)]2+. *Inorg. Chem.* **1998,** *37*, 4838-4848.
66. Mahroof-Tahir, M.; Narasimha Murthy, N.; Karlin, K. D.; Blackburn, N. J.; Shaikh, S. N.; Zubieta, J., New Thermally Stable Hydroperoxo- and Peroxo-Copper Complexes. *Inorg. Chem.* **1992,** *31*, 3001-3003.
67. Itoh, K.; Hayashi, H.; Furutachi, H.; Matsumoto, T.; Nagatomo, S.; Tosha, T.; Terada, S.; Fujinami, S.; Suzuki, M.; Kitagawa, T., Synthesis and Reactivity of a (μ-1,1-Hydroperoxo)(μ-hydroxo)dicopper(II) Complex: Ligand Hydroxylation by a Bridging Hydroperoxo Ligand. *J. Am. Chem. Soc.* **2005,** *127*, 5212-5223.
68. Karlin, K. D.; Ghosh, P.; Gultneh, Y.; Jacobson, R. R.; Blackburn, N. J.; Zubieta, J., Dioxygen-Copper Reactivity: Generation, Characterization, and Reactivity of a Hydroperoxo-Dicopper(II) Complex. *J. Am. Chem. Soc.* **1988,** *110* (20), 6769-6780.

69. Jones, S. M.; Heppner, D. E.; Vu, K.; Kosman, D. J.; Solomon, E. I., Rapid Decay of the Native Intermediate in the Metallooxidase Fet3p Enables Controlled Fe(II) Oxidation for Efficient Metabolism. *J. Am. Chem. Soc.* **2020,** *142* (22), 10087-10101.